imageOwl

TOTAL QA®
Turn Complex to Complete

Improve your test life.

Imagine if you had an integrated QA system that works for you...

Our clients start with an incoherent mix of isolated QA devices, checklists, forms, image processing software, and spreadsheets. As they try to integrate their QA, they are frustrated by systems that won't adapt to their needs.

With Total QA®, they discover a clinically tested, powerful, and customizable service that transforms their machine QA into a coherent whole. With built-in image analysis, custom test templates and a complete API, our clients build QA systems to meet their unique mix of equipment and procedures.

You can improve your test life.
Request a free trial and try it for 3 months free!

Technical Note: Transconvolution based equalization of positron energy effects for the use of ^{68}Ge/^{68}Ga phantoms in determining ^{18}F PET recovery

George A. Prenosil, Michael Hentschel, Markus Fürstner, Thomas Krause, Thilo Weitzel,[a] and Bernd Klaeser
Department of Nuclear Medicine, Inselspital, Bern University Hospital University of Bern, Switzerland

(Received 11 October 2016; revised 21 March 2017; accepted for publication 21 March 2017; published 13 June 2017)

Purpose: Avoiding measurement variability from ^{18}F phantom preparation by using ^{68}Ge/^{68}Ga phantoms for the determination of ^{18}F recovery curves (RC) in clinical quality assurance measurements and for PET/CT site qualification in multicentre clinical trials.
Methods: RCs were obtained from PET/CT measurements of seven differently sized phantom spheres filled either with ^{18}F or with ^{68}Ga. RCs for the respective other isotope were then determined by two different methods: In the first method, images were convolved with positron range transconvolution functions derived from positron annihilation distributions found in literature. This method generated recasted images matching images using the respective other isotope. In the second method, the PET/CT system's isotope independent (intrinsic) point spread function was determined from said phantom measurements and convolved with numerical representations simulating hot spheres filled with the respective other isotope. These simulations included the isotope specific positron annihilation distributions. Recovered activity concentrations were compared between recasted images, simulated images, and the originally acquired images.
Results: ^{18}F and ^{68}Ga recovery was successfully determined from image acquisitions of the respective opposite isotope as well as from the simulations. ^{68}Ga RCs derived from ^{18}F data had a normalized root-mean-square deviation (NRMSD) from real ^{68}Ga measurements of 0.019% when using the first method and of 0.008% when using the second method. ^{18}F RCs derived from ^{68}Ga data had a NRMSD from real ^{18}F measurements of 0.036% when using the first method and of 0.038% when using the second method.
Conclusions: Applying the principles of transconvolution, ^{18}F RCs can be recalculated from ^{68}Ga phantom measurements with excellent accuracy. The maximal additionally introduced error was below 0.4% of the error currently accepted for RCs in the site qualification of multicentre clinical trials by the EARL program of the European Association of Nuclear Medicine (EANM). Therefore, our methods legitimately allow for the use of long-lived solid state ^{68}Ge/^{68}Ga phantoms instead of manually prepared ^{18}F phantoms to characterize comparability of ^{18}F measurements across different imaging sites or of longitudinal ^{18}F measurements at a single PET/CT system. © *2017 The Authors. Medical Physics published by Wiley Periodicals, Inc. on behalf of American Association of Physicists in Medicine.* [https://doi.org/10.1002/mp.12330]

Key words: partial volume effect, PET/CT, positron range function, quantitative imaging, recovery curve, transconvolution

1. INTRODUCTION

Positron emission tomography in combination with computed tomography (PET/CT) is a quantitative clinical imaging modality. Quantifiability of PET/CT, however, suffers from the finite spatial resolution and accordant sampling in the image matrix causing the partial volume effect (PVE) – the spill in and spill out of PET signal to and from adjacent image elements that causes blurring.[1,2]

The PVE of different PET/CT systems is typically determined by phantom measurements: Recovered activity concentrations are typically measured at the center of differently sized hot spheres to compile so called recovery curves (RCs). RC measurements are part of quality assurance (QA) procedures,[3–5] and they constitute an essential element to characterize comparability between different PET/CT systems, e.g., within multicenter clinical trials.[6]

Compared to a ^{18}F filled phantom, which necessitates manual preparation prior to its use, reproducibility of repeated measurements and radiation protection of the performing staff is improved when using a long-lived solid state ^{68}Ge/^{68}Ga phantom (radioactive half-life 270.95 days).[7] However, most clinical images are acquired with ^{18}F-Fluordeoxyglucose (FDG) fluoride anion ($^{18}F^-$) and their RCs cannot be directly compared with those from ^{68}Ga measurements. ^{18}F emits its positron (β^+) with an average energy of 249.8 keV and up to an endpoint energy of 633.5 keV.[8] ^{68}Ga, the daughter nuclide of ^{68}Ge, emits β^+ on average with 836.02 keV and with an endpoint energy of 1899.1 keV.[9] The different isotope energies lead to different source-centred

radial positron annihilation distributions,[10,11] here referred to as positron range functions (PRFs). In PET, the image blur and its consequent PVE will therefore depend on the very isotope used for data acquisition.[12]

Similar to a transconvolution (TC) function (TCF), that conveys images acquired on different PET/CT systems into each other,[13] a positron range transconvolution function (PRTF) can be determined, that conveys ^{18}F measurements into ^{68}Ge measurements ($PRTF_{F\rightarrow Ga}$), or vice versa ($PRTF_{Ga\rightarrow F}$). Akin to Wiener filtering,[14] the PET/CT system's intrinsic PSF (psf_0) acts hereby as a spatial filter against image noise amplification. As described previously, psf_0 is directly determinable from the same phantom acquisitions as the RCs,[15] while necessary PRF models are available from measurements[16] or from computer simulations.[10,11,17]

The $PRTF_{Ga\rightarrow F}$ can then to be applied on ^{68}Ge/^{68}Ga phantom measurements intended for cross-calibrating[18] different PET/CT systems in multicenter clinical trials doing ^{18}F imaging.

Aim of the current work was to prove the feasibility of acquiring ^{18}F RCs from ^{68}Ga phantom measurements and *vice versa*. To this end two strategies were pursued: First, images of hot spheres acquired either with ^{18}F or with ^{68}Ga were transconvolved into images as they would have been acquired with the respective other isotope. Second, ^{18}F and ^{68}Ga RCs were simulated with the PET/CT system's psf_0 and literature derived PRFs. Both, the determination of recovery and of psf_0, were performed on data from the same set of phantom spheres.

1.A. Background and theory

In a given homogenous material, blur from β^+ emitters is solely a function of its positron energy distribution. The annihilation photon's noncollinearity is isotope independent.[19] Thus, knowing a β^+ emitter's energy spectrum, PRF models can be calculated from Monte Carlo (MC) simulations. In this work, the MC derived model provided by J. Cal-González et al.[11] was used with its specific parameters for ^{18}F and ^{68}Ga PRFs. Contrary with others, this model incorporates a maximal positron range r_0, preventing unphysical signal contribution of remote image volume elements (voxels).

Disregarding image noise, a ^{18}F PET/CT image img_F of an object (obj) can be mathematically described by the following Eq.,[20]

$$img_F = obj \circ prf_F \circ psf_0 \tag{1}$$

where $\circ$ denotes convolution. The same holds true for a ^{68}Ga PET/CT image img_{Ga}:

$$img_{Ga} = obj \circ prf_{Ga} \circ psf_0 \tag{2}$$

psf_0 can be deconvolved from PSFs measured either with ^{18}F or ^{68}Ga (psf_F and psf_{Ga}) or estimated directly from a phantom image.[15]

$$psf_0 = psf_F \circ prf_F^{-1} \tag{3}$$

$$psf_0 = psf_{Ga} \circ prf_{Ga}^{-1} \tag{4}$$

According to the convolution theorem, the combined Eqs. (1) and (2) can also be rewritten in Fourier space $\mathcal{F}\{\}$ to arrive at calculated images of a given isotope:

$$\mathcal{F}\left(img_{Ga,calc\ from\ F}\right) = \mathcal{F}(img_F) \times \frac{\mathcal{F}(prf_{Ga})}{\mathcal{F}(prf_F)} \tag{5}$$

$$\mathcal{F}\left(img_{F,calc\ from\ Ga}\right) = \mathcal{F}(img_{Ga}) \times \frac{\mathcal{F}(prf_F)}{\mathcal{F}(prf_{Ga})} \tag{6}$$

The quotients of the two PRFs represents $PRTF_{F\rightarrow Ga}$ in Eq. (5) and $PRTF_{Ga\rightarrow F}$ in Eq. (6), and they act similar to the TCF in an earlier work.[13,21] The main difference here is, that Eqs. (5) and (6) convey between ^{18}F and ^{68}Ga measurements acquired on the same PET/CT system, instead conveying between measurements of the same isotope acquired on different PET/CT systems.

The larger positron spread of ^{68}Ga compared to ^{18}F suppresses high spatial noise in $img_{Ga,calc\ from\ F}$. By contrast, $\mathcal{F}(prf_{Ga})$ drops to naught before $\mathcal{F}(prf_F)$ does (cf. Fig. 1); Eq. (6) will therefore enhance high spatial frequencies, i.e., noise, in $img_{F,calc\ from\ Ga}$. By applying a post hoc low-pass filter with a cut-off frequency f_c, unwanted noise amplification is avoided without compromising quantification in the final filtered image $\tilde{img}_{F,calc\ from\ Ga}$.

This can be shown by examining the corresponding modulation transfer function (MTF) MTF_0 in Fourier space:

$$MTF_0 \equiv |\mathcal{F}\{psf_0\}| \tag{7}$$

The spatial frequency where MTF_0 drops below image noise constitutes the cut-off frequency f_c for *post-hoc* filtering. Here, a 16 pole Butterworth filter with $f_c = 0.25$ mm^{-1} was chosen for its maximally flat pass-band and its steep monotonic gain decay in the spatial frequency domain (MTF_{BW}). Applying the Butterworth filter leads to a filtered calculated image:

$$\mathcal{F}(\tilde{img}_{F,calc\ from\ Ga}) = \mathcal{F}(img_{F,calc\ from\ Ga}) \times MTF_{BW} \tag{8}$$

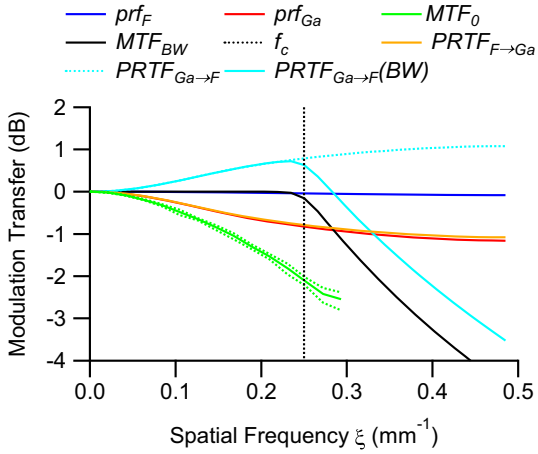

FIG. 1. Modulation transfer of the examined functions plotted as gain in dB. The measured MTF_0 is depicted with ± standard deviation (green dots). The shown MTF_0 was taken from ^{68}Ga data in Ref.15 For clarity, MTF_0 from ^{18}F measurements is not shown.

Figure 1 shows the modulation transfer in decibel (dB) of PRFs, of the Butterworth filter, of PRTFs without filtering, of the PRTF with Butterworth filtering ($PRTF_{Ga\rightarrow F}(BW)$) and of the radial MTF_0 component. No filter is necessary for the TC of ^{18}F images into ^{68}Ga images. It is only used when recasting ^{68}Ga images into ^{18}F images with $PRTF_{Ga\rightarrow F}(BW)$.

2. MATERIAL AND METHODS

2.A. Measurements of recovery curves and point spread functions

Phantom images of seven hot spheres of different diameter and their respective numerical representations were acquired as described previously.[15] The spheres were filled once with ^{18}F and once with ^{68}Ga (200–400 kBq ml^{-1}). Individual sphere images were recorded on a Biograph mCT 128 True-V (Siemens Medical Solutions USA, Knoxville, TN, USA) in time of flight mode (TOF) and reconstructed with filtered back projection into a matrix of 512 × 512 elements using a slice thickness of 1 mm (axial coverage 22.2 cm) in 222 slices. Voxel size was 1.59 mm × 1.59 mm × 1 mm. A post-reconstruction Gaussian filter with a full width half maximum (FWHM) of 2 mm was applied. RCs were determined by measuring the activity concentration in the sphere images at the voxel with the highest intensity. The obtained values were then divided by the expected activity concentration and plotted against sphere diameter.

Numerical representations of the seven hot phantom spheres were calculated at a four times higher resolution than the acquired PET/CT images, and were subsequently Fourier-resampled to the same image matrix as the PET/CT images.

Afterward, psf_0 was individually determined from every sphere for convolution with the respective numerical representation of said sphere filled with the opposite isotope. This approach countered possible nonlinear imaging,[15] in case a PSF not just defines an imaging system but also depends on the diameter of the imaged sphere. The "MTF fit" method[15] was used to establish psf_0. From these individually determined psf_0s it could be shown, that MTF_0 fell near zero after 0.25 mm^{-1}. This value became the subsequently applied f_c (Fig. 1).

Data analysis and all numerical calculations were performed on a HP Z620 Workstation (Palo Alto, CA, USA) running Microsoft Windows 7 as the operating system. Image calculations were run on a multiparadigm Java framework, developed in-house.

2.B. Statistical analysis

For comparing two RCs, RC_a and RC_b, their normalized root-mean-square deviation (NRMSD) was calculated in % as follows:

$$NRMSD = \sqrt{\frac{\sum_i (RC_a(i) - RC_b(i))^2}{n_{spheres}}} \times 100[\%] \quad (9)$$

The number of spheres $\mathbf{n_{spheres}}$ in this work was seven.

3. RESULTS

3.A. Simulation of positron energy effects on recovery

In order to understand the influence of the isotope's different positron ranges onto recovery, numerical representation of spheres (*obj*) were convolved with PRFs to simulate hot spheres with their individual positron reach (obj_F and obj_{Ga}).

$$obj_F = obj \circ prf_F \quad (10)$$

$$obj_{Ga} = obj \circ prf_{Ga} \quad (11)$$

Plotting RCs from simulated obj_F and obj_{Ga} (Fig. 2) reveals that the positron induced spread from ^{18}F has no effect on the recovery of activity concentration from spherical objects in the chosen size range. By contrast, a drop was observed in the simulated ^{68}Ga RC around the 1 ml sphere, i.e., for objects with Ø <12.4 mm.

Convolving the same data with an additional simulated Gaussian three dimensional PSF with 6 mm full width at half maximum (FWHM) produced differences between the two isotopes already at the 4 ml sphere. In this case, ^{68}Ga experienced a sharp drop in recovery for spheres with a volume <2 ml (Fig. 2, dotted lines). The RC from *obj* convolved with the Gaussian PSF was, by any practical means, congruent with the RC from obj_F convolved with the Gaussian PSF (Data not shown).

Solid lines in Fig. 2 show RCs acquired from ^{18}F and ^{68}Ga measurements of single hot spheres of different diameters (img_F and img_{Ga}). Note that the two measured curves show a distinct displacement, even though the same set of spheres and identical acquisition parameters were used for both isotopes. The difference necessitates normalization factors as followed in Section 3.B which does not impede the method.

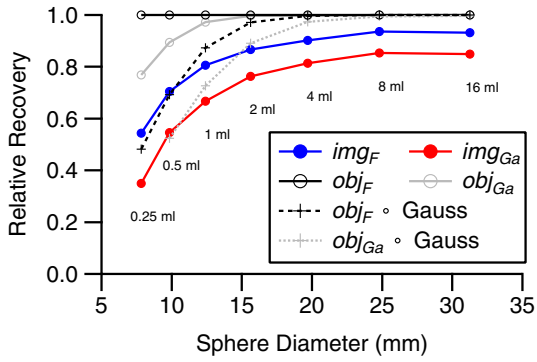

FIG. 2. RCs of seven spheres measured with ^{18}F (blue) and ^{68}Ga spheres (red), and simulated RCs of *obj* with prf_F (black) and prf_{Ga} (gray). Dotted black and grey lines represent convolution with an additional simulated Gaussian PSF with 6 mm FWHM. Recovery is normalized to the true activity concentration in the spheres. Black numbers below the curves indicate sphere volumes.

3.B. Recovery curves from real transconvolved measurements

To test the eligibility of $PRTF_{F\rightarrow Ga}$ to convey ^{18}F measurements into ^{68}Ga measurements we convolved the imaged ^{18}F spheres with $PRTF_{F\rightarrow Ga}$ according to Eq. (6), arriving at $img_{Ga,calc\ from\ F}$. All measurements were normalized to the recovery of their largest 16 ml spheres. To do so for ^{18}F measurements, said normalization factor was 1.073. For ^{68}Ga measurements the normalization factor was 1.177. The normalization factors seem to stem from the measurement setup's deviating calibrations for the different isotopes (cf. Discussion). Figure 3(a) depicts resultant RCs and their congruence with the measured ^{68}Ga curves from Fig. 2. NRMSD between those two was 0.019%.

The convolution of $PRTF_{Ga\rightarrow F}(BW)$ [Eq. (8)] with the imaged ^{68}Ga spheres gave. Their recovery is also shown together with the measured ^{18}F recovery in Fig. 3(a). NRMSD between those two RCs was 0.036%.

3.C. Recovery curves from numerical representations of phantom spheres

To test, if a PET/CT systems psf_0 can be used as substitute for real phantom measurements with a particular isotope, $psf_{0,Ga}$ determined directly from the ^{68}Ga phantom images of Ref. [15] was convolved with obj_F. The radial FWHM of $psf_{0,Ga}$ was 4.9 ± 0.1 mm. The thereof determined RC had a NRMSD of 0.008% from the img_{Ga} RC. Next, $psf_{0,F}$ determined from ^{18}F phantom measurements was convolved with obj_{Ga}. The radial FWHM of $psf_{0,F}$ was 4.8 ± 0.2 mm. The hereof determined RC had a NRMSD of 0.038% from the img_{Ga} RC. Simulated normalized RCs are shown in Fig. 3(b).

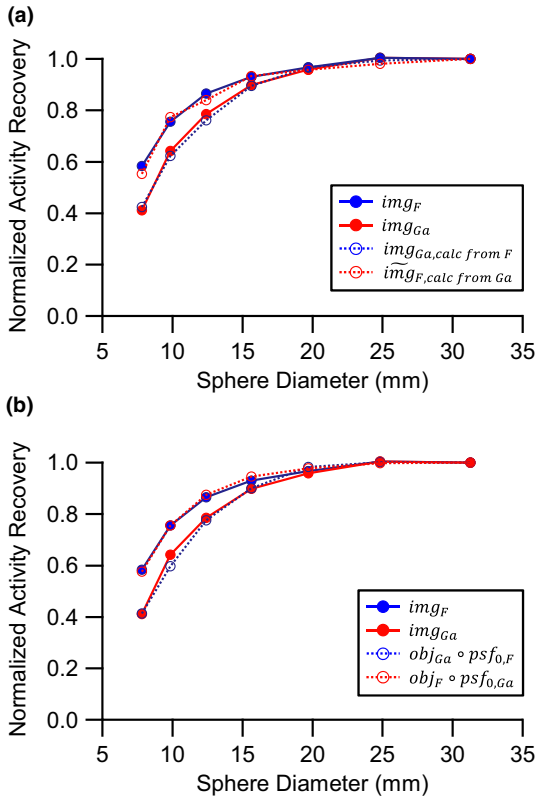

FIG. 3. RCs from transconvolved imaged spheres (a) and from simulated spheres convolved with psf_0 (b) compared with measured RCs (solid lines). Recovery is normalized to the recovery seen in the largest sphere. Blue lines depict RCs obtained solely from ^{18}F measurements, whereas red lines depict RCs obtained solely from ^{68}Ga measurements.

4. DISCUSSION

Two strategies were applied to generate RCs of a particular PET isotope from data acquired with a different isotope. The first strategy transconvolved real PET/CT images of single spheres into images of the opposite isotope. The second strategy used the PET/CT system's intrinsic psf_0 to simulate sphere images of the two different isotopes. Both strategies were able to convey normalized RCs for an isotope based on measurements using the respective other isotope. Only the factor mending the displacement between the two curves needed to be established with the respective isotopes.

Gaussian filters as applied in Fig. 2 are widely used in clinical routine. The simulation of accordant RCs showed, that positron energy effects need to be considered when imaging structures smaller than 15 mm.

From

$$\mathcal{F}(prf_F)(\xi) \rightarrow 1, \xi < \xi_c \tag{12}$$

follows that prf_F has small effects on PET/CT clinical measurements compared to prf_{Ga}. Therefore, it can be accepted that for most cases

$$\frac{\mathcal{F}(prf_{Ga})}{\mathcal{F}(prf_F)} \approx \mathcal{F}(prf_{Ga}) \tag{13}$$

Within the physical limits set by the clinical imaging system,[22,23] any such derived $PRTF_{F\rightarrow Ga}$ will represent an approximation of $\mathcal{F}(prf_{Ga})$, rendering additional filtering superfluous (cf. Fig. 1). The absent influence of obj_F on recovery supports this view (Fig. 2).

As shown by Fig. 3(a), determining img_{Ga} from ^{18}F acquisitions is trivial. In this case simulated ^{18}F RCs were more accurate than RCs from $img_{Ga,calc\ from\ F}$; probably because any object specific imaging bias introduced by the PET/CT system was accounted for by determining psf_0 for every sphere anew.

^{18}F RCs from transconvolved ^{68}Ga measurements had a worse NRMSD from actual ^{18}F RCs, compared to ^{68}Ga RCs from transconvolved ^{18}F measurements. Here, the remaining high spatial frequency amplification of $PRTF_{Ga\rightarrow F}(BW)$ resulted in a noisier $img_{F,calc\ from\ Ga}$. In this case, simulations were equally capable of determining ^{18}F RCs from ^{68}Ga measurements as from.

Common eligibility criteria given by EARL for the participation in multicenter clinical trials have NRMSD values of 9.7% (SUV_{max}) and 5.8% (VOI-A50) for their margin of

error in RC measurements.[6,24] This is about 260 times more than our novel method will introduce to the data.

In general, any deviation between calculated and measured recovery curves are attributed most likely to measurement variability. Similarly, fluctuations in simulated RCs are caused by the residual inaccuracy when determining psf_0 or MTF_0 (Fig. 1).

Using a dedicated ^{68}Ge/^{68}Ga phantom in lieu of ^{18}F phantoms should result, together with the proposed methodology for RC determination, in smaller measurement errors, in more reproducible data and in lower radiation exposure.[25] When using our second approach of RC calculations from simulated spheres [Fig. 3(b)], determining psf_0 is enough to fully describe a PET/CT system. That is, no actual recovery curves had to be measured at all, and the isotope used for imaging is included post-hoc. Use of this method is warranted, when determining psf_0 with a different method other than using measurements on hot spheres.[13,15] However, the normalization factor between ^{18}F and ^{68}Ga measurements needs to be determined separately, ideally with the use of large cylindrical phantoms. From previous calibration experiments with a homogeneous hot cylinder phantom of 200 mm diameter and 6.28 l volume we had found normalization factors of 1.01 for ^{18}F and of 1.19 for ^{68}Ga. The similarity to the herein reported normalization factors (cf. Results) also confirms, that at a sphere volume of >16 ml full recovery is reached in the sphere center. Such a sphere can thus be used for RC normalization for clinical PET/CT systems with FWHMs around 6 mm.

The normalization factor compensates for the perceived differences in activity concentration between the stock solutions of the two different isotopes and the activity concentration in acquired PET/CT images. This disparity can stem from imprecise calibrations of the activimeter used for the original preparation or from different measurement geometries.

Disadvantages include additional costs of the dedicated ^{68}Ge/^{68}Ga phantom. Also, ^{18}F RCs derived from these measurements show some, albeit small, noise amplification. Here, a proper choice of the Butterworth filter is mandated.

5. CONCLUSION

Dedicated ^{68}Ge/^{68}Ga phantoms can replace the commonly used ^{18}F phantoms for RC and psf_0 determination in clinical routine,[7] even when ^{18}F RCs are requested. The advantages of reproducibility and safe handling as well as lower radiation exposure and reduced workload for the staff justify the additional expenditure of having a dedicated ^{68}Ge/^{68}Ga solid state phantom. Following above outlined procedures will allow the use of a single ^{68}Ge/^{68}Ga solid state phantom for site qualification in multicenter clinical trials or for longitudinal bias measurements on a single PET/CT system.[26] Concurrent use of ^{18}F and ^{68}Ga phantoms at different PET/CT sites is also conceivable.

When using a ^{68}Ge/^{68}Ga phantom in multicenter clinical trials, determination of the participating PET/CT systems' psf_0 is advisable over psf_F or psf_{Ga}. The correspondent isotope specific *prf* can then be easily incorporated into the PSF or TCF. The data can then be normalized with the transconvolution method.

ACKNOWLEDGMENTS

Thanks to the staff at the Department of Nuclear Medicine, Inselspital Bern, for assistance with the PET phantom measurements.

CONFLICTS OF INTEREST

The authors have no relevant conflicts of interest to disclose.

[a)]Author to whom correspondence should be addressed. Electronic mail: thilo.weitzel@insel.ch; Telephone (+41)3163-20868.

REFERENCES

1. Hoffman EJ, Huang SC, Phelps ME. Quantitation in positron emission computed tomography: 1. Effect of object size. *J Comput Assist Tomogr*. 1979;3:299–308.
2. Soret M, Bacharach SL, Buvat I. Partial-volume effect in PET tumor imaging. *J Nucl Med*. 2007;48:932–945.
3. N.E.M. Association. *NEMA Standards Publication NU 2-2012: Performance Measurements of Positron Emission Tomographs*. Rosslyn, VA: NEMA National Electrical Manufacturers Association; 2012.
4. Boellaard R. Standards for PET image acquisition and quantitative data analysis. *J Nucl Med*. 2009;50:11S–20S.
5. Boellaard R, Oyen W, Hoekstra C, et al. The Netherlands protocol for standardisation and quantification of FDG whole body PET studies in multi-centre trials. *Eur J Nucl Med Mol Imaging*. 2008;35:2320–2333.
6. Boellaard R. *New EANM FDG PET/CT Accrediation Specifcations for SUV Recovery Coefficients*. Vienna: EARL European Association of Nuclear Medicine; 2011.
7. Kinahan P, Doot R, Christian P, et al. Multi-center comparison of a PET/CT calibration phantom for imaging trials. *J Nucl Med*. MEETING ABSTRACTS 2008;49:63.
8. Tilley DR, Weller HR, Cheves CM, Chasteler RM. Energy levels of light nuclei A = 18–19. *Nucl Phys A*. 1995;595:1–170.
9. McCutchan EA. Nuclear data sheets for A = 68. *Nucl Data Sheets*. 2012;113:1735–1870.
10. Jødal L, Loirec CL, Champion C. Positron range in PET imaging: an alternative approach for assessing and correcting the blurring. *Phys Med Biol*. 2012;57:3931.
11. Cal-González J, Herraiz JL, España S, et al. Positron range estimations with PeneloPET. *Phys Med Biol*. 2013;58:5127.
12. Levin CS, Hoffman EJ. Calculation of positron range and its effect on the fundamental limit of positron emission tomography system spatial resolution. *Phys Med Biol*. 1999;44:781–799.
13. Prenosil GA, Weitzel T, Hentschel M, Klaeser B, Krause T. Transconvolution and the virtual positron emission tomograph – A new method for cross calibration in quantitative PET/CT imaging. *Med Phys*. 2013;40:062503–062517.
14. Norbert W. *Extrapolation, Interpolation, and Smoothing of Stationary Time Series*. New York: Wiley; 1949.
15. Prenosil GA, Klaeser B, Hentschel M, et al. Isotope independent determination of PET/CT modulation transfer functions from phantom measurements on spheres. *Med Phys*. 2016;43:5767–5778.
16. Derenzo SE. Precision measurement of annihilation point spread distributions for medically important positron emitters. 5th International Conference on Positron Annihilation, Lake Yamanaka, Japan, April 8-11, 1979, LBNL Paper LBL-9169.

17. Wirrwar A, Vosberg H, Herzog H, Halling H, Weber S, Muller-Gartner HW. 4.5 tesla magnetic field reduces range of high-energy positrons-potential implications for positron emission tomography. *Nucl Sci IEEE Trans*. 1997;44:184–189.
18. Weitzel T, Corminboeuf F, Klaeser B, Krause T. Kreuzkalibrierung von positronen-emissions-tomographen für multizentrische studien: Festkörper-phantom und transconvolution. *SGSMP-Bulletin*. 2010;72:9–13.
19. DeBenedetti S, Cowan CE, Konneker WR, Primakoff H. On the angular distribution of two-photon annihilation radiation. *Phys Rev.* 1950;77:205–212.
20. Fellgett PB, Linfoot EH. On the assessment of optical images. *Philos Trans R Soc Lond A*. 1955;247:369–407.
21. Weitzel T, Prenosil GA, Hentschel M, Klaeser B, Krause T. Response to 'Comment on 'Transconvolution and the virtual positron emission tomograph (vPET): a new method for cross calibration in quantitative PET/CT imaging. *Med Phys*. 2013;40:15.
22. Siemens, Biograph™ Inside Biograph TruePoint PET•CT. edited by M. Siemens AG, DE, www.healthcare.siemens.com/molecular-imaging (2008).
23. Herraiz JL, España S, Vicente E, Vaquero JJ, Desco M, Udias JM. Noise and physical limits to maximum resolution of PET images. *Nucl Instrum Methods Phys Res, Sect A*. 2007;580:934–937.
24. Fahey FH, Kinahan PE, Doot RK, Kocak M, Thurston H, Poussaint TY. Variability in PET quantitation within a multicenter consortium. *Med Phys*. 2010;37:3660–3666.
25. Lockhart CM, MacDonald LR, Alessio AM, McDougald WA, Doot RK, Kinahan PE. Quantifying and reducing the effect of calibration error on variability of PET/CT standardized uptake value measurements. *J Nucl Med*. 2011;52:218–224.
26. Doot RK, Pierce LA, Byrd D, Elston B, Allberg KC, Kinahan PE. Biases in multicenter longitudinal PET standardized uptake value measurements. *Trans Onc*. 2014;7:48–54.